

JOSIP JURAJ STROSSMAYER UNIVERSITY OF OSIJEK
FACULTY OF ELECTRICAL ENGINEERING, COMPUTER SCIENCE
AND INFORMATION TECHNOLOGY OSIJEK

INSTRUMENTATION AMPLIFIERS FOR THE
MEASUREMENT OF BIOSIGNALS

BACHELOR'S DEGREE FINAL PROJECT

Author: **Victor Šimić de Torres**
Supervisor: **Tomislav Matić PhD.**

“Invention is the most important product of man's creative brain. The ultimate purpose is the complete mastery of mind over the material world, the harnessing of human nature to human needs”. Nikola Tesla

ABSTRACT

The instrumentation amplifiers for measuring biological signals have been evolving exponentially in recent years, since the first publication of a capacitively-coupled chopper instrumentation amplifier. This amplifier opened the door to a brand-new way to amplify biological signals, growing in accuracy and, above all, in noise cancellation efficiency.

The following thesis presents the instrumentation amplifiers fundamentals, providing the state-of-the-art review on the advanced instrumentation amplifiers architectures. The aim of this project is to design an instrumentation amplifier circuit suitable for the measurement of electromyography (EMG) signals. Therefore, this thesis presents the fundamentals of human body biosignals with emphasize on the EMG, acquisition of EMG signal and the implemented analog front-end circuit for EMG signal measurement.

Following the Introduction in chapter 1, the thesis provides fundamentals on electromyography in chapter 2. The EMG measurement circuit description is provided in chapter 3, including the simulation results. Detailed specification of the implemented prototype for EMG measurement is provided in chapter 4. Chapter 5 presents the measurement results, followed by the concluding remarks in chapter 6.

RESUM

Els amplificadors d'instrumentació (IA) per a la mesura de senyals biològiques han estat evolucionant ràpidament en els darrers anys des de la publicació del primer CCIA. Aquest amplificador va obrir la porta a una nova manera d'amplificar senyals biològiques, amb més precisió i, sobretot, més eficiència en tant a l'absorció de soroll.

Aquest projecte estudia primer els fonaments dels amplificadors d'instrumentació, fent una revisió del “*State-of-the-art*” en les arquitectures avançades dels amplificadors d'instrumentació. L'objectiu d'aquest projecte és dissenyar un circuit IA adequat per a la mesura de senyals electromiogràfiques (EMG). Per això, aquest projecte presenta els fonaments dels biosenyals en el cos humà fent èmfasi en el EMG, adquisició de senyal EMG i el circuit analògic front-end implementat per a mesura de senyal EMG.

Seguint a la introducció al capítol 1, aquesta tesi proveeix fonaments en electromiografia en el capítol 2. La descripció del circuit de mesura EMG es troba al capítol 3, inclosos els resultats de la simulació. L'especificació detallada del prototip implementat per mesura EMG es proveeix al capítol 4. El capítol 5 presenta els resultats mesurats, seguit per les conclusions al capítol 6.

RESUMEN

Los amplificadores de instrumentación (IA) para medida de bioseñales han estado evolucionando rápidamente en los últimos años desde la primera publicación del CCIA. Este amplificador abrió la puerta a toda una nueva manera de amplificar señales biológicas, con mayor precisión y, sobre todo, eficiencia en absorción de ruido.

Este proyecto estudia primero los fundamentos de los amplificadores de instrumentación, haciendo una revisión del “*State-of-the-art*” en las arquitecturas más avanzadas de los amplificadores de instrumentación. El objetivo de este proyecto es diseñar un circuito IA adecuado para la medida de señales electromiográficas (EMG). Con ese objetivo, este proyecto presenta los fundamentos de los bioseñales en el cuerpo humano enfatizando en el EMG, la adquisición de señal EMG y el circuito front-end analógico implementado para la medida de señal EMG.

Siguiendo a la introducción en el capítulo 1, esta tesis provee de los fundamentos en elecromiografía en el capítulo 2. La descripción del circuito de medida EMG se encuentra en el capítulo 3, incluidos los resultados de la simulación. La especificación detallada del prototipo implementado para la medida EMG se provee en el capítulo 4. El capítulo 5 presenta los resultados medidos, siguiendo las conclusiones en el capítulo 6.

ACKNOWLEDGEMENTS

I would like to thank my supervisor, Tomislav Matić, for guiding me in through my thesis and Damir Rukavina for helping me when I was building the prototype.

Also, I would like to thank my new friends from Erasmus and my old friends at home for all the patience when I explained this project to them, knowing that they didn't understand electronics.

Finally, I want to thank my family who has supported and encouraged me from the day I knew I wanted to become an engineer.

Thank you for all the support.

TABLE OF CONTENTS

ABSTRACT.....	2
RESUM.....	3
RESUMEN.....	4
ACKNOWLEDGEMENTS.....	5
TABLE OF CONTENTS	6
1. INTRODUCTION.....	7
1.1 BIOMEDICAL SIGNALS.....	7
1.2 INSTRUMENTAL AMPLIFIERS GENERAL OVERVIEW.....	7
1.3 USES OF IAs IN BIOMEDICAL ENGINEERING.....	8
1.4 STATE OF THE ART OF IAs FOR BIOSIGNALS MEASUREMENT.....	10
2. ELECTROMYOGRAPHY	13
2.1 SURFACE ELECTROMYOGRAPHY (sEMG).....	13
3. DESIGN OF A CIRCUIT FOR sEMG.....	15
3.1 PARTS OF THE DESIGN.....	15
3.1.1 PREAMPLIFIER STAGE.....	15
3.1.2 BANDPASS FILTER	15
3.1.3 LAST STAGE AMPLIFIER.....	18
3.2 SIMULATION.....	19
4. CONSTRUCTION OF THE CIRCUIT	21
4.1 MATERIAL	21
4.2 DEVELOPMENT OF THE CIRCUIT	22
4.2.1 BREADBOARD	22
4.2.2 PCB	22
5. RESULTS	24
5.1 AC ANALYSIS	28
6. BUDGET.....	32
7. CONCLUSIONS.....	33
8. KEY WORDS	34
9. BIBLIOGRAPHY	35
ANNEX 1.....	37

1. INTRODUCTION

1.1 BIOMEDICAL SIGNALS

A biomedical signal is considered to be any signal in living beings that can be continually measured and analyzed, mostly referred to bioelectrical signals. This thesis will focus on an electromyogram, which is defined as the electrical potential generated by the working muscles.

1.2 INSTRUMENTAL AMPLIFIERS GENERAL OVERVIEW

The instrumentation amplifiers (IAs) are differential amplifiers with input buffer stages. Just like operational amplifiers (Op Amp), IAs can be used in a close-loop as gain blocks whose amplitude at the output is controlled by the feedback resistors. The main difference between Op Amps and IAs is the higher immunity of the IAs to the noise between the inputs (because of the subtraction of the signals). The internal structure of the IAs is provided in the Figure 1. The presented IA has two buffers at the input (one per each input) and a differential amplifier, the output is referred to ground potential.

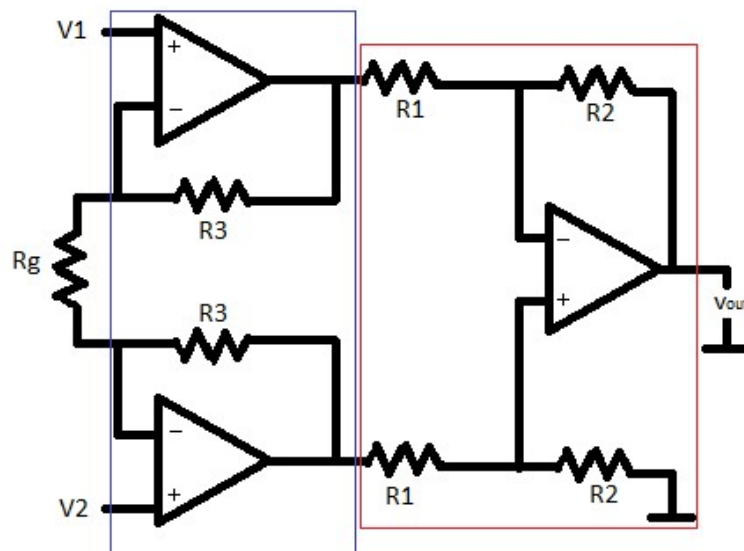


Figure 1. The structure of a three operational IA. The blue zone shows the two buffers and the red zone highlights the differential amplifier. The Rg is the resistance used to control the gain.

The differential amplifier is used to subtract one signal to the other, making the operation $V1-V2$. This operation is important in order to attenuate the common noise between the

signals, and this is the main reason why IAs are used in instrumentation applications. The formula for the gain of the amplifier in Figure 1 is (1.1).

$$V_{Out} = \frac{\left(1 + \frac{2R_3}{R_g}\right)R_2}{R_1} \quad (1.1)$$

The amplifier from the Figure 1 is one of the most basic examples of IA architecture. Depending on the required application, there is a wide range of different IAs architectures that have been designed to achieve particular characteristics. One of many examples is the current feedback IA (CFIA), which uses current sensing in order to increase the CMRR. The conventional resistive feedback IA, such as the one shown in Figure 1, requires matched resistors with high precision to achieve a high CMRR, while the CFIA shows high CMRR and better power efficiency [1]. But even with all of these advantages, the CFIA comes with certain drawbacks. For example, the gain accuracy in the CFIA is determined by the match between the input and the feedback transconductor which is signal dependent. Apart from that, there is a subclassification of the CFIA, depending on if it is using direct current or indirect current. Direct current CFIA has been traditionally used in low power biomedical applications because its main advantage is a reduced current dissipation, while indirect current CFIA has been traditionally used in analog front-end circuits for biomedical applications. Despite the drawbacks of CFIA, there are several biomedical designs that put into use this type of IA, for example, [2] proposes a circuit that makes CFIA suitable to be used in electroencephalogram (EEG) detection systems. Advanced IAs with improved properties will be explained in later sections of this thesis.

1.3 USES OF IAs IN BIOMEDICAL ENGINEERING

As explained in the previous subsection, the instrumental amplifiers are very useful for measuring weak signals in a noisy environment. This is the main reason why the use of an IA is absolutely necessary to acquire signal from the human body. Every signal that comes from the living beings is affected by other signals that are not the one of interest and represent a noise. Therefore, it is essential to use filters to remove any frequency that is not the one of interest.

In the field of the biomedical engineering, the instrumentational amplifier is required to have following characteristics: a high input impedance, to minimize the effect of the measurement to the signal, a low output impedance (for the same reason), a limited bandwidth to adjust the signals of interest, and a low power consumption. Also, it must have an adequate gain to reach the maximal gain without arriving to saturation, high power-supply rejection ratio (PSRR) and CMRR [3]. Biomedical signals normally have

an amplitude of few millivolts (mV), even reaching the order of the microvolts (μV), and a range of frequencies is very limited, so the aim is to amplify the signal until it reaches the order of hundreds of millivolts and to cut all the frequencies outside the range of interest.

In order to design an amplifier according to the parameters explained above, there are several examples to build a circuit that manages to accomplish the most important aspects for the accuracy of the system, like the ones appearing in [3], that improves the input offset voltage by an offset cancellation technique, and [4], that proposes an IA built in three stages that accomplishes high CMRR, high PSRR and low RMS input noise. In 2007 the capacitively-coupled chopper instrumentation amplifier (CCIA) was published [5], [6], intended to be used in electrocardiography and electroencephalography, but its use has been extended in most of the branches looking for biomedical signals acquisition. The main reasons for its expansion were all the benefits of this kind of IA which, as explained in [5] has:

- Outstanding DC input Common Mode (CM) isolation: The virtual ground of the Op Amp is isolated from common-mode DC voltages at the input. That is possible because of an input capacitor (C_{in}). Because of that, a rail-to-rail input CM voltage range (CMVR) can be obtained if the chopper at the input of the Op Amp can handle it.

- Great noise efficiency: The noise in CCIAs mainly comes from the Op Amp, so the fact that it only uses single Op Amp, makes the CCIA way more efficient in comparison to the classical three operational IA architecture (the one that appears in Figure 1).

- High gain accuracy: The gain in CCIAs is equal to the ratio C_{in} / C_{fb} (Figure 2), which increases the amplification accuracy.

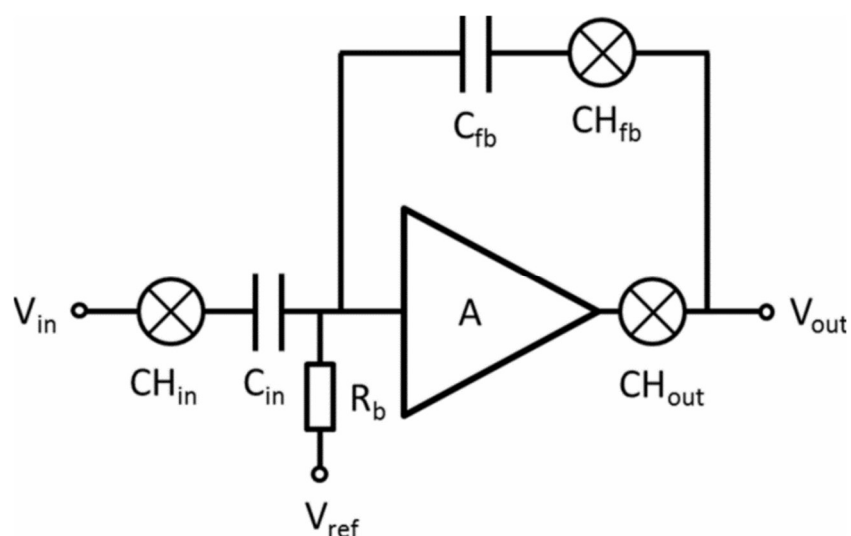


Figure 2. The circuit of the basic CCIA. The “A” is the Op Amp, which has the single input terminal and the other terminal connected to V_{ref} . The CH blocks are chopper blocks [5].

Despite several advantages, CCIA's also come with big disadvantages (as explained in [5]):

-Relatively low input-impedance: It can be approximated with the formula $1/2f_{chop}C_{in}$ where f_{chop} is the frequency of the chopper at the input (C_{Hin}). This is a problem in most of the biomedical applications, because as mentioned before, for measuring biological signals it is important to have a high input impedance.

-High-impedance biasing: To avoid a great contribution to the noise, a large impedance biasing is required, but this high impedance slows down the settling time of the CCIA virtual ground. The order of these impedances usually requires implementation by pseudo-resistors.

-Very sensitive to large signal CM interference: Large AC CM signals can pass through C_{in} and appear at the input of the Op Amp distorting the signal.

To reduce the effect of those disadvantages, the original CCIA evolved into different types, depending on the required performances. For example, if the aim is to improve the input impedance (some biomedical applications need an input impedance around Giga Ohms and the CCIA only reaches the Mega Ohms), Positive Feedback Loop (PFL) can be used [5]. The design is quite simple, because it consists just of a chopper and a feedback capacitor, and the noise influence to the circuit as well as the power consumption are both negligible. The objective of the feedback loop is to reduce the input current since the ideal value of the input current for the CCIA is equal to 0. Due to parasitic capacitances and the stability of this circuit, the effectivity is limited. To achieve high impedance biasing reducing a noise, reference [7] uses duty-cycle resistors in place of large resistors. On average, the equivalent resistor value is proportional to the ratio $1/D$, so just by changing the duty-cycle factor it is possible to control the resistor value. This type of resistor is more reliable than the pseudo-resistor when the order of magnitude is over $10\text{ G}\Omega$ [7]. Furthermore, the use of duty-cycle method shows a better noise performance compared to the pseudo-resistors.

1.4 STATE OF THE ART OF IAs FOR BIOSIGNALS MEASUREMENT

Choosing the correct instrumentation amplifier is vital for the efficiency of biomedical signals acquisition. That is the reason why one of the most popular instrumentational amplifiers for biopotential recording is the capacitively-coupled instrumentation amplifier (CCIA) with particular modifications to adapt the properties to be suitable for measurement of particular signals [5], [8]. Along the past decade (since 2007) a huge

contribution has been reported in the field of the biopotentials measurement. This thesis will provide the review of relevant examples of applications of IAs for biopotentials recording. The Current-Mode Capacitively-Coupled Chopper Instrumentation Amplifier (C^4IA) [9] for recording neuronal signals, will be explained further.

The C^4IA is a solution that was founded to outcome the drawbacks of a biopotential acquisition analog front-end (AFE). Typically, a CCIA is used in the biopotential AFE to reduce input referred noise (IRN) and to block the DC signals that may distort the output. Also, it needs large servo loops (as in the design in [8]) or coupling capacitors to minimize the $1/f^2$ IRN or the offset voltage induced by the chopper [10]. All of this limits the channel density, when the neural recording devices needs to increase the channel density aiming to track simultaneously the activity of large population of neurons [9].

To minimize the noise from the capacitively-coupled AFE, [9] uses input coupling capacitors and chopper-stabilization without having large chopper-induced IRN or servo loops. This can be done because it places the chopper after the coupling capacitor but outside the feedback loop of the first amplifier, so the structure becomes a current mode amplifier. Then, after the amplification, it uses a capacitive integrator to turn back to voltage mode, and the signal gets digitized using an ADC ending as a complete AFE that offers low-noise/power and occupies low area [9]. Figure 3 shows these three stages in a schematic of the C^4IA . The C^4IA also allows chopping with capacitive coupling in an area-efficient manner, not like the regular AC-coupled chopper-stabilized architectures, that need large capacitors for the same low noise and stability [9].

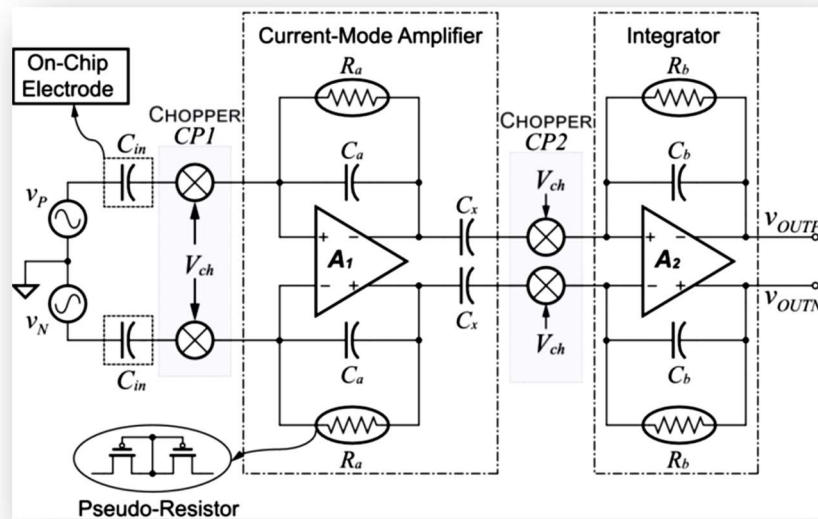


Figure 3. The circuit of the C^4IA , proposed in [9].

Nevertheless, this is just one of the CCIA improvements over the past years. In another example, [11] proposes a way to reduce the ripple at the output for electroencephalography (EEG), electrocardiography (ECG) and neural recording, without using the usual filters that add phase delay. To circuit from [11] is provided in the Figure 4. The circuit reduces the ripple which is accomplished with the use of two capacitors in the main signal path that blocks DC and ping-pong autozeroing technique [11]. Similar approach is a circuit built into two identical stages and proposed by [12] that work inversely, because while one of the stages is amplifying the other is autozeroing. However, the input impedance of the CCIA is very low, as it is one of the three great drawbacks in this kind of IA, and this circuit needs an input impedance of minimum 50 M Ω [11]. The solution implemented in [11] is an impedance boosting loop, built in the feedback loop of the first stage to be able to increase the input impedance to 100 M Ω .

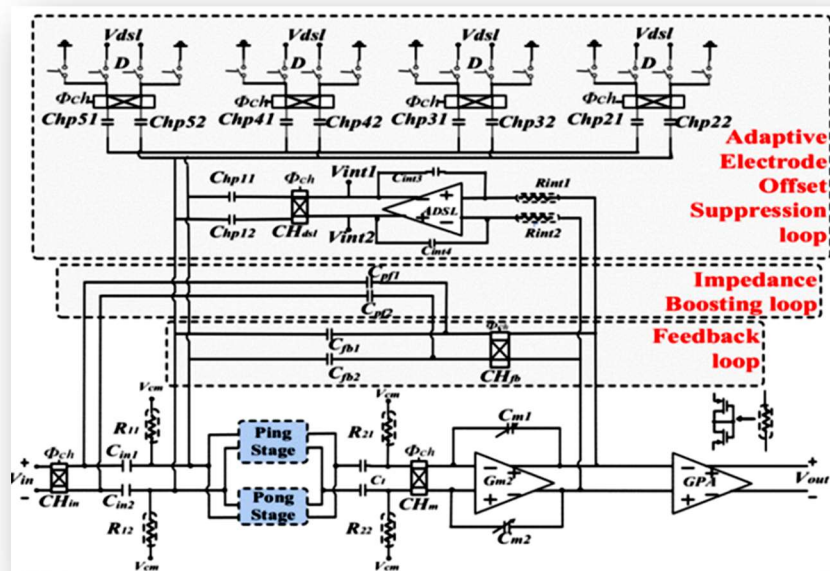


Figure 4. Schematic of the circuit proposed by [11] for reducing the ripple in the output of the CCIA.

2. ELECTROMYOGRAPHY

Electromyography (EMG) is an experimental technique developed to analyze the bioelectrical signal produced by skeletal muscles. There are two types of EMG measurements regarding the electrodes that are used:

- The intramuscular needle: It is an invasive method where the electrode is a needle that is placed inside the muscle. This ensures the selectivity to the fiber muscle due to its size, and allows to measure either superficial or profound muscles. It is characterized by having a high signal-noise ratio, so it allows to have a wide frequency range.
- The surface electromyography (sEMG): It is a non-invasive method where the electrodes are placed on the surface of the skin. It allows a global register of the muscle activity and it only works with superficial muscles. Also, the frequency range of this technique is relatively small, because even when the real range of frequency is between 20 and 500 Hz, the signal is dominant just between 50 and 150 Hz [13]. This is the reason why in the circuit design for this thesis the parameters for the bandpass filter will be in the second range, just to be able to acquire the dominant signal.

In this thesis the aim is to design and construct the circuit for a sEMG using the instrumentation amplifier and the filters.

2.1 SURFACE ELECTROMYOGRAPHY (sEMG)

The sEMG signal is a bioelectrical signal that can be recorded via electrodes and exists along with the contraction of the muscles. As explained previously, the range of the sEMG signal is found between 20 Hz and 500 Hz. Its amplitude is concentrated between 0 and 5 millivolts (mV), normally between 0.01 mV and 5 mV [13]. This amplitude usually is within the noise level, so in order to acquire the signal, it is required to amplify the signal and remove the noise to ensure the correct measurement. That means that the circuit needs to have a high input impedance, a low output impedance, a high gain accuracy, a high CMRR and a low noise [3], [13].

The major advantage of this technique is that it is non-invasive, safe, real time and relatively easy to implement. The terms “real time” and “non-invasive” are two of the most important ones, because it means that it is possible to measure the sEMG signal and the state of the muscle in the patient in real time and for a required amount of time, with the less discomfort for the user. However, the amount of time that the patient can have the electrodes on the skin is limited, because the electrodes are on the skin, affected by the sweat, sebum or large range of motion [14] which can take them out or distort the signal. Also, the sEMG has the disadvantage that it works just on superficial muscles.

Leaving aside the examples of sEMG application, like in medicine, to determine the state of some of the skeletal muscles (one of the most well-known diagnosis with sEMG is the carpal tunnel syndrome), there are other application areas of sEMG. One example is proposed by [14] that analyzes the gesture using a sEMG. The paper proposes a new type of analysis that rises the accuracy of the detection to 74.7 % [14].

Another example of sEMG application is [15] that proposes a robot to assist the mobility. The idea is that the robot works as a new kind of mobility tool that improves the live quality of the people with walking disabilities [15]. The main idea is that it can work either with android phone control or with sEMG in the arm muscles. In the paper [15], the authors show that the robot accepts simple orders like forward, backwards, turn right and turn left. Another use case of sEMG application is in prosthesis for people who lost the upper limbs. The sEMG is used to recognize the intention of the patient to control the prosthetic arm. Although the prosthetic arms of this kind are expensive [16], there are several works targeting to make this kind of prosthesis accessible at lower costs.

3. DESIGN OF A CIRCUIT FOR SEMG

As explained in the introduction, the most suitable amplifier for measuring biological signals, should be one of the CCIA. The CCIA can be efficiently implemented in integrated circuit, which is the main reason why the IA designed for this thesis is the classical three operational IA, that is possible to implement using Commercial Of The Shelf (COTS) components. The IA will be followed by a bandpass filter of 6th order, in which the lower cutoff frequency will be 50 Hz and the upper cutoff frequency will be 150 Hz. Despite the fact that the whole range of EMG frequencies is from 20 Hz to 500 Hz, this thesis will limit to cut-off the frequency spectrum outside the spectrum of dominant sEMG signals. After the filter stage, the amplifier will be implemented to enable additional amplification of the signal.

3.1 PARTS OF THE DESIGN

As explained in [17], the basic parts of a biopotential amplifier are a preamplifier, a high pass filter, an isolation amplifier and a low pass filter. In this thesis, the chosen preamplifier architecture is the three Op Amp based instrumentation amplifier (Figure 1), the high pass filter and the low pass filter, united in an active bandpass filter without an isolation amplifier, but with the amplifier in the last stage that will enable to adjust the required gain. In the following sub-sections, each part of the design will be explained.

3.1.1 PREAMPLIFIER STAGE

In this thesis the aim was to explore the instrumentation amplifiers, and for that reason the IA will be implemented using COTS components. According to the circuit from the Figure 1, if R1, R2 and R3 have equal resistance, the original equation for the gain (1.1) becomes (3.1):

$$V_{Out} = 1 + \frac{2R}{R_g} \quad (3.1)$$

The IA will be made of three OP07 (datasheet in [19]), with six resistors of 27k Ω , and the resistor R_g value is 1k Ω . Accordingly, the gain is equal to 55.

3.1.2 BANDPASS FILTER

As explained before, the implemented bandpass filter is a 6th order bandpass active filter. The gain of the filter is set at 10 because the signal in the sEMG can vary between 10 μ V and 5 mV [13] and the aim is to amplify the signal and use the whole range that the amplifier can withstand without arriving to saturation.

The implemented filter is a multiple feed-back bandpass filter (MFB) of 6th order. That is achieved using three MFB of 2nd order simultaneously [18]. The approximation used in this thesis is Butterworth, because the frequency cutoff is sharper than the Bessel, but yet it does not have the ripple of the Chebyshev in the step response.

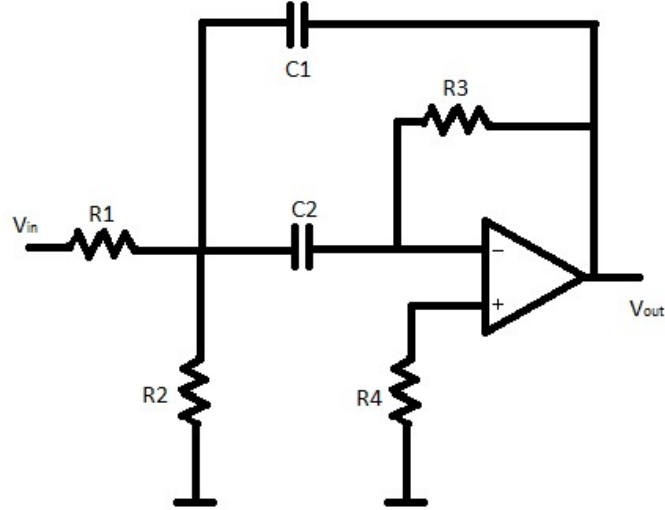


Figure 5. The MFB bandpass filter circuit.

The equations (3.2) to (3.6) are used for the design of the filter and the designer can choose freely C_1 :

$$R_1 = \frac{Q_{BP}}{2\pi f_0 A C_1} \quad (3.2)$$

$$R_2 = \frac{1}{4\pi f_0 Q_{BP} C_1} \quad (3.3)$$

$$R_3 = R_4 = \frac{\left(\frac{Q_{BP}^2}{Q_{BP}^2 + A} + 1\right) Q_{BP}}{2\pi f_0 C_1} \quad (3.4)$$

$$C_2 = \left(\frac{A}{Q_{BP}^2} + 1\right) C_1 \quad (3.5)$$

$$Q_{BP} = \frac{f_0}{f_h - f_L} \quad (3.6)$$

“A” represents the total gain of the active passband filter, “ f_0 ” is the central frequency (the middle between the high cutoff and the low cutoff), “ Q_{BP} ” is the quality factor for the bandpass filter, “ f_h ” denotes the cutoff in the high frequencies and “ f_L ” the cutoff in the low frequencies. For designing the 6th order bandpass filter, three MFB bandpass

filter stages are used, which means that for each stage it is necessary to find the Q_{BP} , the A and the f_0 . For that objective, the following equations are used (accessible in [18]):

$$Q_{BPx} = Q_{BPy} = \sqrt{\frac{\left(k_{LP}^2 + 4Q_{BP}^2 + \sqrt{(k_{LP}^2 + 4Q_{BP}^2)^2 - \frac{4k_{LP}^2 Q_{BP}^2}{Q_{LP}^2}}\right)}{\frac{2k_{LP}^2}{Q_{LP}^2}}} \quad (3.7)$$

$$f_{0x} = \frac{f_0}{\frac{k_{LP} Q_{BPx}}{2Q_{LP} Q_{BP}} + \sqrt{\left(\frac{k_{LP} Q_{BPx}}{2Q_{LP} Q_{BP}}\right)^2 - 1}} \quad (3.8)$$

$$f_{0y} = f_0 \left(\frac{k_{LP} Q_{BPy}}{2Q_{LP} Q_{BP}} + \sqrt{\left(\frac{k_{LP} Q_{BPy}}{2Q_{LP} Q_{BP}}\right)^2 - 1} \right) \quad (3.9)$$

$$A_x = A_y = \sqrt[n]{A^2} \sqrt{1 + Q_{BPx}^2 \left(\frac{f_0}{f_{0x}} - \frac{f_{0x}}{f_0}\right)^2} = \sqrt[n]{A^2} \sqrt{1 + Q_{BPy}^2 \left(\frac{f_{0y}}{f_0} - \frac{f_0}{f_{0y}}\right)^2} \quad (3.10)$$

$$Q_{BPz} = \frac{Q_{BP}}{k_{LP}} \quad (3.11)$$

$$f_{0z} = f_0 \quad (3.12)$$

$$A_z = \sqrt[n]{A^2} \quad (3.13)$$

The equations (3.7) to (3.10) are vital to design an MFB bandpass filter, if the order is superior to 2. For a bandpass filter of 2nd order, equations (3.11) to (3.13) are sufficient to define the parameters. If the filter order is superior to 2nd order, but it cannot be implemented using an even number of bandpass filters, it will be necessary to use all equations from (3.7) to (3.13), since in the case of an uneven number of filters, the paired ones will follow the equations (3.7) to (3.10) and the unpaired one will follow the equations (3.11) to (3.13).

In the equations (3.7) to (3.13), the sub-index “x”, “y” and “z” are used to identify which filter is referring to, “x” and “y” are the paired ones and “z” is the unpaired one. The “n” in the formulas (3.10) and (3.13) represents the order of the filter, and the Q_{LP} and the k_{LP} are the factors acquired from the table in annex 1, the table of the approximation of Butterworth low pass filters of high order.

In the case of the implementing a filter, as explained before, as the 6th order bandpass filter, which is made of an uneven number of filters, in order to design the filter all, the equations from (3.7) to (3.13) are required. The first two filters follow the equations (3.8) to (3.10) and the third one follows the equations (3.11) to (3.13). To design this filter, the

first step is to go to the table in annex 1 and search for the Q_{LP} and k_{LP} values for a 3rd order lowpass filter. A 6th order bandpass filter is made of a 3rd order lowpass filter and a 3rd order high pass filter. The results are as follow, taking in account that the parameters of the filter are a cutoff frequency of 50 Hz in the low frequency and 150 Hz in the high frequency (following the formula (3.6) the total Q_{BP} is 1), and a gain equal to 10:

$$Q_{BP1} = Q_{BP2} = 2.1889 \quad (3.14)$$

$$f_{01} = 64.9679 \text{ Hz} \quad (3.15)$$

$$f_{02} = 153.9222 \text{ Hz} \quad (3.16)$$

$$A_1 = A_2 = 4.7158 \quad (3.17)$$

$$Q_{BP3} = 1; f_{03} = 100 \text{ Hz}; A_3 = 2.1544 \quad (3.18)$$

Taking into account all of these parameters, it is possible to build the bandpass filter. Since it is possible to choose the C1 value in each filter, the components were chosen to achieve the minor difference between the calculated component values and the standard ones. Based on the value of the capacitor C1, for which the capacitor C2 showed the minor error, the resistor values are chosen.

3.1.3 LAST STAGE AMPLIFIER

As explained before, the signal in the sEMG ranges between 10 μV and 5 mV. That makes difficult to adjust the total gain and to use the entire voltage range using the predefined filter gain. That is the reason why this amplifier has been set at the output of the circuit to allow additional amplification, if needed. The design of this amplifier is an inverting amplifier (Figure 6), and the gain is defined by the equation (3.19). According to the equation (3.19), it is possible to adjust the total gain by proper choice of the resistors R1 and R2.

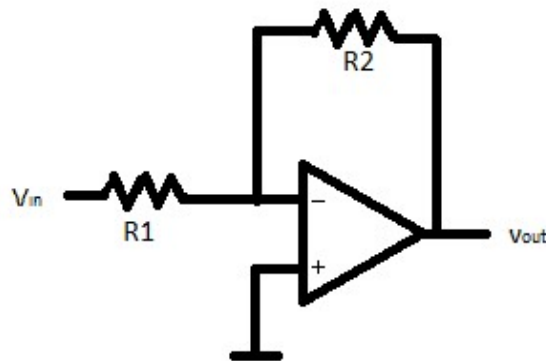


Figure 6. Inverting amplifier. The gain in this amplifier follows the formula (3.19)

$$V_{Out} = -\frac{R2}{R1}V_{in} \quad (3.19)$$

For the design, the resistors values have been adjusted to $R1=10k\Omega$ and $R2=10k\Omega$, with unity gain and amplifier acting as a voltage follower and impedance transformer.

3.2 SIMULATION

The simulation of the circuit is performed using LTSpice XVII, and for the sake of an accurate simulation, all the operational amplifiers used in the simulation are real OP07 [19] models, the ones that will be used for practical implementation of the circuit. As it can be seen in the Figure 7, the amplifiers are supplied with a voltage of $\pm 15V$. At the same time in Figure 7 it is possible to see that all the resistors and capacitors have standard values, to enable simple implementation of the circuit, except the two capacitors, whose values are equal to 12.2 nF. These capacitors will be implemented, using two capacitors in parallel, one of 10nF and another of 2.2 nF.

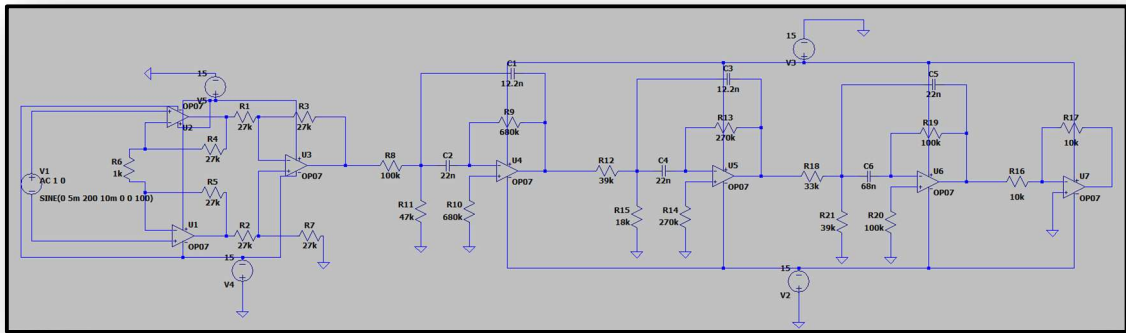


Figure 7. Circuit designed via LTSpice XVII with all the stages (preamplifier, filter and amplifier).

The Figure 8 shows the ac simulation results for the circuit model from the Figure 7. It is possible to see that the filter is attenuating 60 dB per decade on both sides, as expected for a 6th order bandpass filter. Even if originally the circuit was meant to attenuate between 50 Hz and 150 Hz, the obtained attenuation (-3 dB) is found between 60 Hz and 160 Hz, but it is an expected deviation due to approximation of all the components to enable use of the standard component values. However, even in that case the obtained signal bandwidth should be satisfactory for the sEMG. The most important point in this filter is that it needs to attenuate less than 20 Hz and more than 500 Hz, where most of the signals are regarded as a noise.

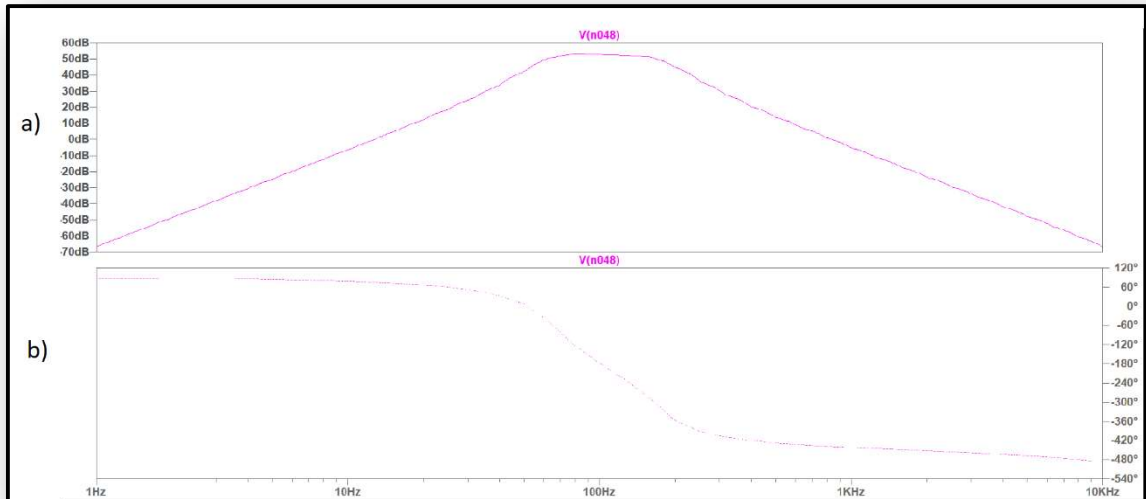


Figure 8. AC response of the circuit in Figure 7. The parameters of the simulation: 10 points per decade, 1Hz as start frequency and 10kHz as stop frequency. The upper graph, Figure 8 a), shows the gain in dB while the lower graph, Figure 8 b), shows the phase in degrees.

4. CONSTRUCTION OF THE CIRCUIT

After designing the circuit, the next step is the construction. The design is implemented on the breadboard to minimize the potential corrections of the PCB.

4.1 MATERIAL

The bill of material in the design includes following components:

Operational Amplifiers:

7 – OP07. The datasheet of this Op Amp can be founded in [19]. Each OP 07 has only 1 Op Amp.

Capacitors:

2 – 2.2 nF

2 – 10 nF

3 – 22 nF

1 – 68 nF

Resistors:

1 – 1 k Ω

2 – 10 k Ω

1 – 18 k Ω

6 – 27 k Ω

1 – 33 k Ω

2 – 39 k Ω

1 – 47 k Ω

3 – 100 k Ω

2 – 270 k Ω

2 – 680 k Ω

Other Components:

7 – Socket for Op Amps

2 – T. Block connector with 3 inputs

1 – T. Block connector with 2 inputs

4.2 DEVELOPMENT OF THE CIRCUIT

After designing the circuit and defining the components, the next step is testing the circuit in the breadboard before PCB design. The breadboard is used to test the designed filter and amplifier and to measure the bandwidth and the gain of the circuit.

4.2.1 BREADBOARD

Following the Figure 9, the circuit from the Figure 7 was implemented from down to top and from left to right, placing the output on the upper right side of the breadboard and the input on the lower left side of the breadboard. The amplifier at the output of the circuit has unity gain, both of the resistors having value of $10\text{ k}\Omega$. The test circuit in the breadboard has confirmed that the design is in line with the requirements.

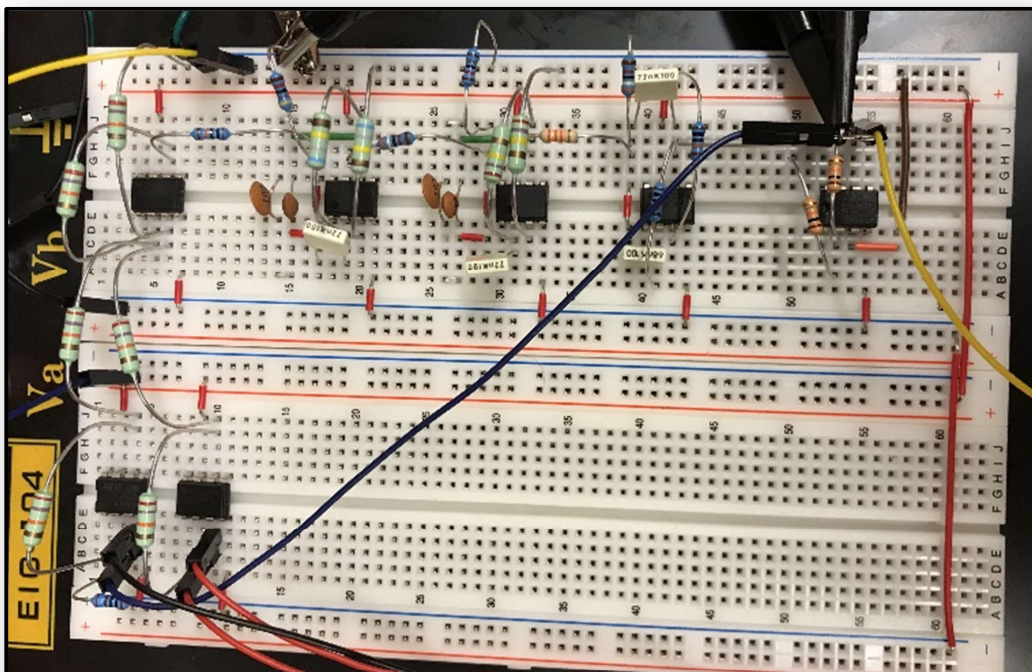


Figure 9. The breadboard implementation of the circuit.

4.2.2 PCB

After confirmation of the design accuracy in the breadboard, the PCB (Printed Circuit Board) design is being initiated. The circuit is implemented using a two-layer PCB board. Figure 10 and Figure 11 show the upper and the bottom layer of the PCB respectively. As it is possible to see, on the top side of the PCB the inputs and the power supply of the circuit are placed on the left side of the board, the Op Amps are placed in corresponding

sockets and on the right side of the resistors is the output. Finally, at the bottom part of PCB the capacitors are placed.



Figure 10. Upper layer of the PCB

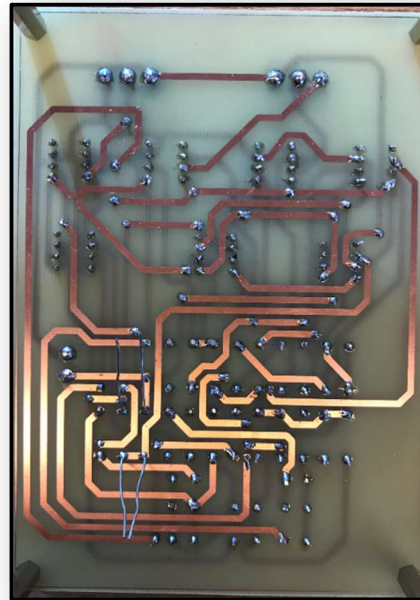


Figure 11. Bottom layer of the PCB

5. RESULTS

The main functionality of the designed circuit is to register the sEMG signals. For that purpose, the chosen skeletal muscle to register sEMG signal was the biceps. The measurement setup requires three electrodes: two for the differential inputs and the third one for the reference ground.

Figure 12 shows the sEMG inputs, outputs and the power supply connection of the circuit. At the left part of the picture, the t. block on top is the power supply input, red wire for +15V, black for -15V and green for ground. The t. block at the bottom is for the connection of the electrodes mounted on the arm. The red and the black are used for the differential inputs, and the yellow for the reference ground. Lastly, at the top of the circuit there is the output, for measurement of the output signal using an oscilloscope, the red wire is the output node, while the green one is the ground reference.

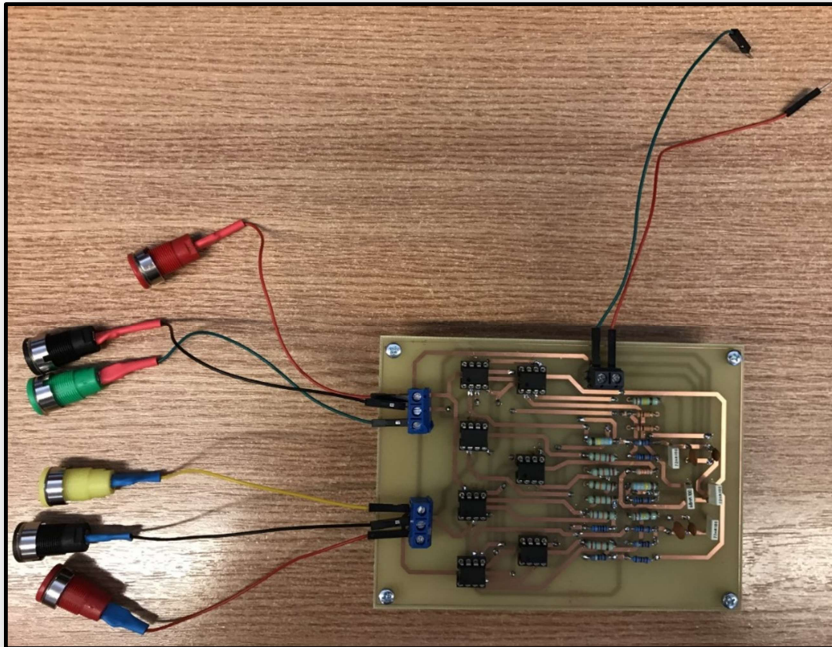


Figure 12. The designed PCB for sEMG signal measurement.

Following the color code for the electrodes in Figure 12, Figure 14 and Figure 15 shows the movements of the arm in order to register a change in the signal at the output, while Figure 13 denotes the different locations where the electrodes will be placed in order to register the signal from the biceps. The movements are the flexion and extension of the arm, and the expected result is a change in the voltage at the output.

The movement of flexion will suppose contraction of the biceps while extension represent the relaxation. During the contraction of the biceps, the electrical activity of the muscle will be recorded.

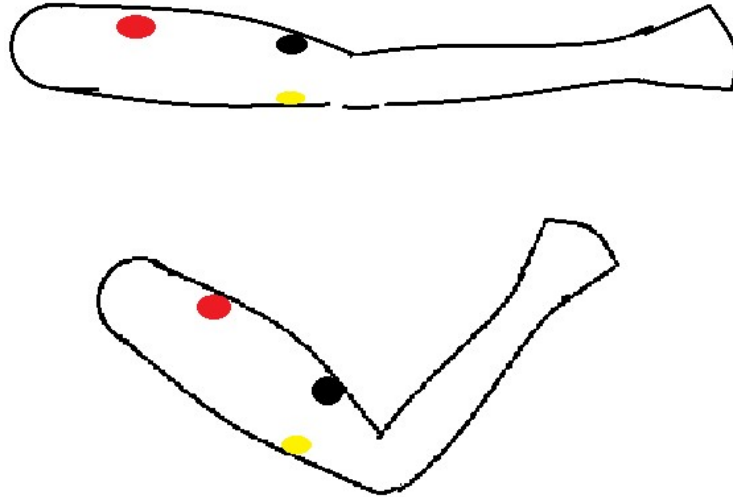


Figure 13. Drawing of the arm movements. The color dots represent the electrodes, and follow the color code in Figure 12.



Figure 14. Contracting the biceps

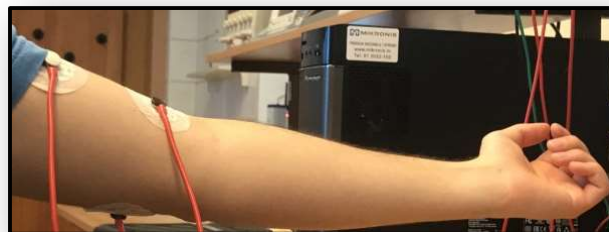


Figure 15. Relaxing the biceps

As explained previously, the expected results are a change in the voltage at the output while moving the arm as shown in the Figure 13. The resulting waveforms are presented in Figure 16, Figure 17 and Figure 18. The acquired signal represents the recording of the muscle activity in the expected frequency range. Figure 14 shows the result obtained when the arm was in extension, with a peak when flexing the arm. The oscilloscope was set to 10 mV/DIV (millivolts per division), so the results are that the output when the arm is in flexion reaches around 25 mV peak-peak.

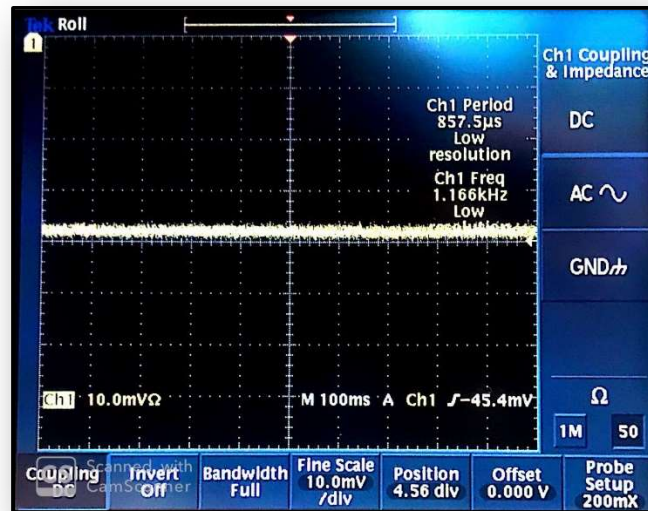


Figure 16. The registered signal when the biceps is in extension (Figure 15).

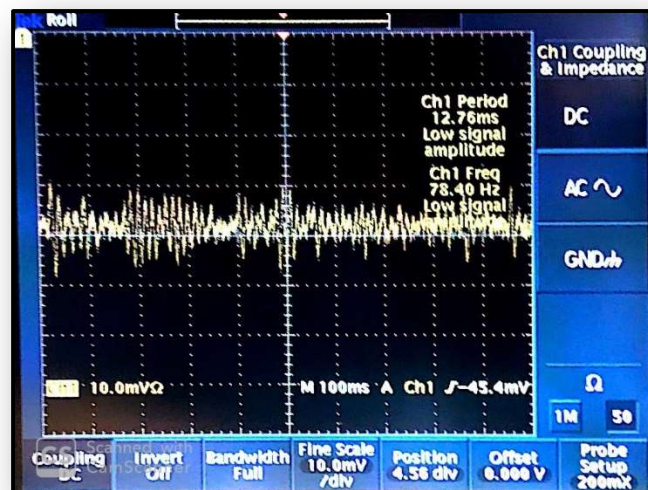


Figure 17. Registered signal when the arm is in flexion (Figure 14).

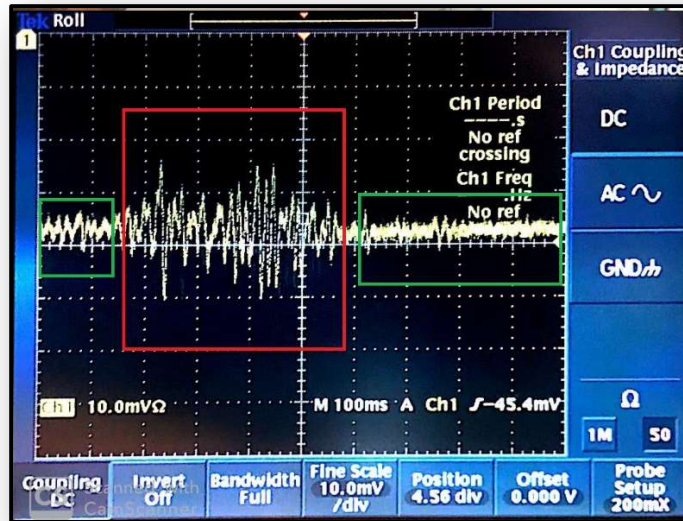


Figure 18. This picture shows the change between the two states. The red part shows the arm in flexion while the green parts shows the results of the extension.

5.1 AC ANALYSIS

The AC analysis is performed, in order to compare it with the simulation results.

The AC analysis was performed taking the points between 1 and 300 Hz. At each frequency, the total gain of the circuit was measured. To enable more accurate comparison of the measured and simulated results, the simulation results in Figure 19 were obtained using the same parameters as for the measurements.

For the analysis in Figure 20, the resultant gain in dB is calculated using the equation (5.1), where U_{IN} is the amplitude of the input voltage (for the analysis it was 10 mV), while the U_{OUT} is the amplitude of the output voltage.

$$V(dB) = 20\text{Log}_{10}\left(\frac{U_{OUT}}{U_{IN}}\right) \quad (5.1)$$

As it can be seen, the measurement and simulation results in Figure 19 a) and Figure 20 have good agreement. However, there is a significant difference in attenuation at low frequencies and the constant gain in the bandwidth of interest is lower in the Figure 20 compared to the gain from the Figure 19. The mismatch in the measurement and simulation results is caused by the different characteristics of the real components and simulation models. The noise contribution, including the power supply noise, additionally deteriorates the measurement results.

Figure 19 b) and Figure 21 represent the simulated and measured phase-frequency characteristics of the circuit. As is possible to see, the measured phase-frequency characteristic shows good match with the simulated results.

The characteristics in Figure 20 and Figure 21 are obtained from the measurement results provided in the Table 1.

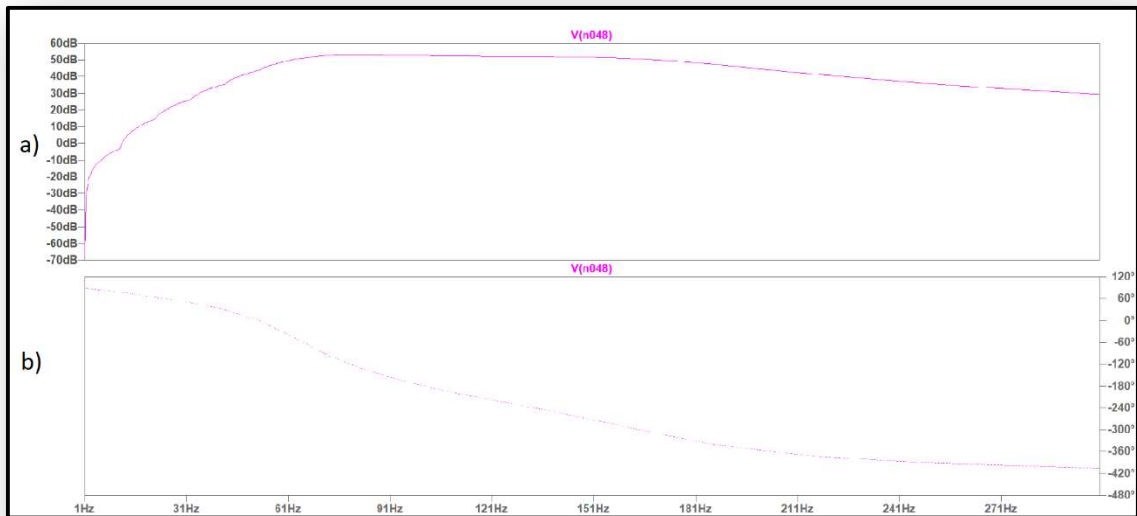


Figure 19. Amplitude-frequency (a) and phase-frequency (b) characteristics of the circuit in Figure 7. The parameters of the simulation: 30 pints, 1Hz as start frequency and 300 Hz as stop frequency.

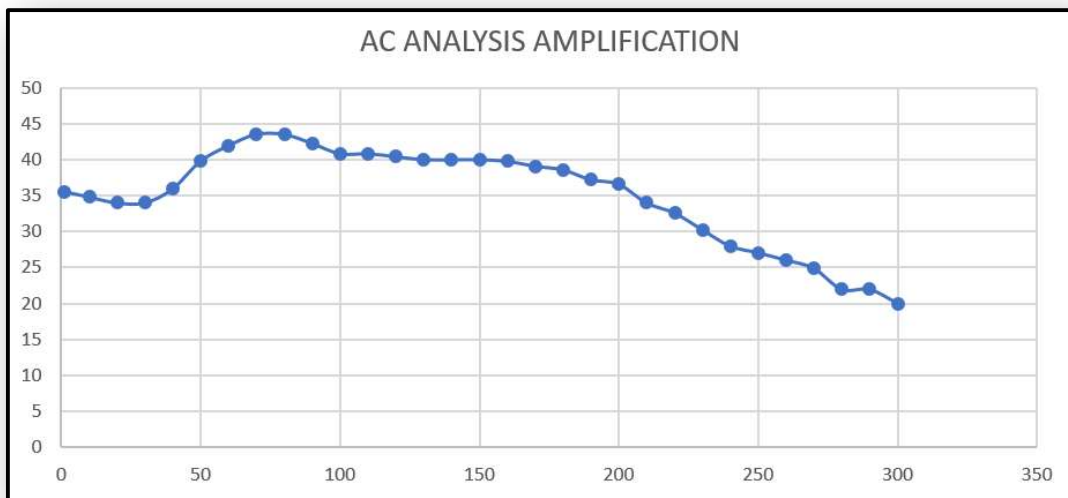


Figure 20. The measured amplitude frequency characteristic. The ordinate axis is in dB while the abscissa axis is in Hz

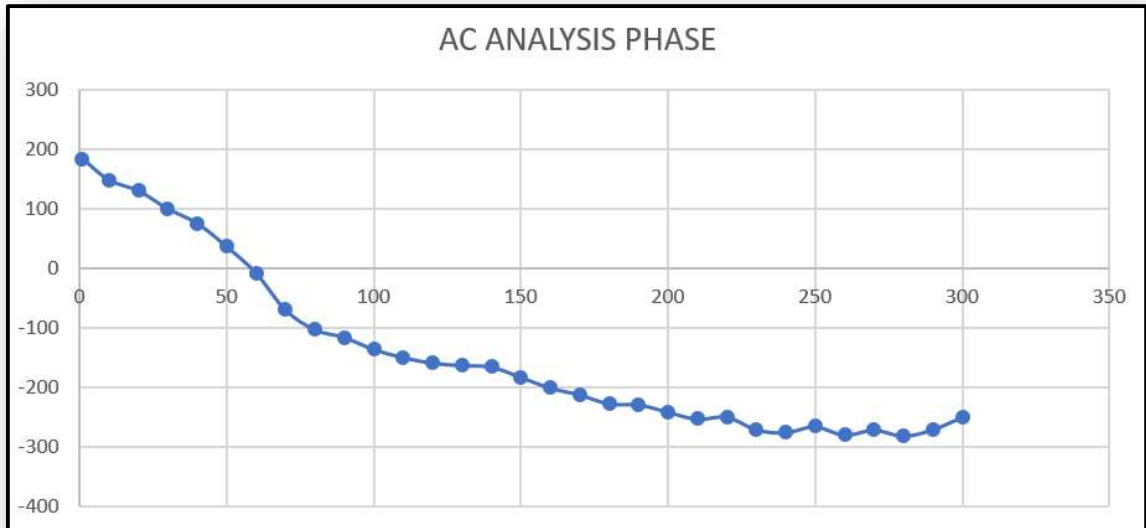


Figure 21. The measured phase-frequency characteristic. The ordinate axis is in degrees while the abscissa axis is in Hz

Table 1. The measurement results for amplitude-frequency and phase-frequency characteristics from Figure 20 and Figure 21

INPUTS		OUTPUTS			
Frequency (Hz)	Voltage (V)	Voltage (V)	Gain	Gain (dB)	Phase, degrees
1	0.01	0.6	60	35.563025	183.6
10		0.55	55	34.8072538	147.6
20		0.5	50	33.9794001	129.6
30		0.5	50	33.9794001	99.36
40		0.625	62.5	35.9176003	74.88
50		0.975	97.5	39.7800923	36
60		1.25	125	41.9382003	-8.64
70		1.5	150	43.5218252	-70.56
80		1.5	150	43.5218252	-103.68
90		1.3	130	42.278867	-116.64
100		1.1	110	40.8278537	-136.8
110		1.1	110	40.8278537	-150.48
120		1.05	105	40.423786	-159.84
130		1	100	40	-163.8
140		1	100	40	-166.32
150		1	100	40	-183.6
160		0.975	97.5	39.7800923	-201.6
170		0.9	90	39.0848502	-212.976
180		0.85	85	38.5883785	-228.096
190		0.725	72.5	37.2067601	-229.824
200		0.675	67.5	36.5860755	-241.92
210		0.5	50	33.9794001	-254.016
220		0.425	42.5	32.5677786	-250.272
230		0.325	32.5	30.2376672	-271.584
240		0.25	25	27.9588002	-276.48
250		0.225	22.5	27.0436504	-266.4
260		0.2	20	26.0205999	-280.8
270		0.175	17.5	24.860761	-272.16
280		0.125	12.5	21.9382003	-282.24
290		0.125	12.5	21.9382003	-271.44
300	0.1	10	20	-250.56	

6. BUDGET

The bill of material for the designed circuit, including the quantities and price of the components is provided in the Table 2.

Table 2. The bill of material

MATERIAL	AMOUNT	PRICE (kn)		PRICE (€)	
		ONE	TOTAL	ONE	TOTAL
OP 07	7	9	63	1.20	8.40
Sockets	7	2.5	17.5	0.33	2.33
Resistors	21	0.3	6.3	0.04	0.84
Breadboard	1	134.9	134.9	17.99	17.99
Double sided PCB	1	20	20	2.67	2.67
Ceramic Capacitors	4	0.9	3.6	0.12	0.48
Plastic Capacitors	4	1.5	6	0.20	0.80
T. Block	3	3	9	0.40	1.20
TOTAL			260.3		34.71

7. CONCLUSIONS

The thesis describes the fundamentals of the IA architectures, providing the recent state-of-the-art in the field of IAs for biopotential recordings with emphasis on the EMG signals, more particularly sEMG signals. In line with the proposed circuit for sEMG measurement, the simulation results are provided, justified by the measurement results in the final chapter.

The circuit implemented in this thesis is aimed for recording biomedical signals, more particularly sEMG signal. Due to a required accuracy for the biomedical signals recording, and owing to the chosen three Op Amp based IA implementation, the proposed circuit uses a high order filter at the output of the IA. The obtained results justify the functionality of the designed circuit for the measurement of sEMG signal.

8. KEY WORDS

ADC: Analog to Digital Converter.

AFE: Analog Front-End.

Bandwidth

CCIA: Capacitively-coupled chopper instrumentation amplifier.

CFIA: Current Feedback Instrumentation Amplifier.

CMRR: Common-Mode Rejection Ratio.

CMVR: Common-Mode Voltage Range.

ECG: Electrocardiography.

EEG: Electroencephalography.

EMG: Electromyography

IA: Instrumentation Amplifier

IC: Integrated Circuit.

IRN: Input Referred Noise.

Noise

Op Amp: Operational Amplifier.

PSRR: Power Supply Rejection Ratio.

sEMG: Surface Electromyography

9. BIBLIOGRAPHY

- [1] Wu, R., Huijsing, J., & Makinwa, K. (2011). A Current-Feedback Instrumentation Amplifier With a Gain Error Reduction Loop and 0.06% Untrimmed Gain Error. *IEEE Journal Of Solid-State Circuits*, 46(12), 2794-2806. doi: 10.1109/jssc.2011.2162923
- [2] Mahmoud, S., & Alhammadi, A. (2015). A CMOS CFIA with digitally controlled gain designed for EEG systems. 2015 International Soc Design Conference (ISOC). doi: 10.1109/isocc.2015.7401638
- [3] Yen, C., Chung, W. and Chi, M. (2004). Micro-Power Low-Offset Instrumentation Amplifier IC Design for Biomedical System Applications. *IEEE Transactions on Circuits and Systems I: Regular Papers*, 51(4), pp.691-699.
- [4] Wang, C., Huang, C., Liou, J., & Fang, K. (2006). A 140-dB CMRR Low-noise Instrumentation Amplifier for Neural Signal Sensing. *APCCAS 2006 - 2006 IEEE Asia Pacific Conference On Circuits And Systems*. doi: 10.1109/apccas.2006.342102
- [5] Fan, Q., & Makinwa, K. (2018). Capacitively-coupled Chopper Instrumentation Amplifiers: An Overview. 2018 IEEE SENSORS. doi: 10.1109/icsens.2018.8589958.
- [6] T. Denison, K. Consoer, W. Santa et al., "A 2 μ W 100nV/ $\sqrt{\text{Hz}}$ chopper stabilized instrumentation amplifier for chronic measurement of neural field potentials", *IEEE JSSC*, vol. 42, no. 12, pp. 2934-2945, Dec. 2007.
- [7] Chandrakumar, H., & Markovic, D. (2016). 5.5 A 2 μ W 40mVpp linear-input-range chopper- stabilized bio-signal amplifier with boosted input impedance of 300M Ω and electrode-offset filtering. 2016 IEEE International Solid-State Circuits Conference (ISSCC). doi: 10.1109/isscc.2016.7417924
- [8] Zheng, J., Ki, W., Hu, L., & Tsui, C. (2017). Chopper Capacitively Coupled Instrumentation Amplifier Capable of Handling Large Electrode Offset for Biopotential Recordings. *IEEE Transactions On Circuits And Systems II: Express Briefs*, 64(12), 1392-1396. doi: 10.1109/tcsii.2017.2741348
- [9] Wang, H., & Mercier, P. (2018). A Current-Mode Capacitively-Coupled Chopper Instrumentation Amplifier for Biopotential Recording With Resistive or Capacitive Electrodes. *IEEE Transactions On Circuits And Systems II: Express Briefs*, 65(6), 699-703. doi: 10.1109/tcsii.2017.2780171
- [10] Song, H., Park, Y., Kim, H., & Ko, H. (2015). Fully Integrated Biopotential Acquisition Analog Front-End IC. *Sensors*, 15(10), 25139-25156. doi: 10.3390/s151025139
- [11] Zhou, Y., Zhao, M., Dong, Y., Wu, X., & Tang, L. (2018). A Low-Power Low-Noise Biomedical Instrumentation Amplifier Using Novel Ripple-Reduction Technique. 2018 IEEE Biomedical Circuits And Systems Conference (Biocas). doi: 10.1109/biocas.2018.8584744

- [12] Chong-Gun Yu, & Geiger, R. (1994). An automatic offset compensation scheme with ping-pong control for CMOS operational amplifiers. *IEEE Journal Of Solid-State Circuits*, 29(5), 601-610. doi: 10.1109/4.284713
- [13] Liu, J., An, C., Hu, A., & Lv, S. (2018). Modular Simulation Teaching of Analog Electronic Technology Based on sEMG Signal Acquisition Circuit. 2018 International Conference On Information Systems And Computer Aided Education (ICISCAE). doi: 10.1109/iciscae.2018.8666907
- [14] Xiong, A., Zhang, D., Zhao, X., Han, J., & Liu, G. (2014). Classification of Gesture based on sEMG Decomposition: A Preliminary Study. *IFAC Proceedings Volumes*, 47(3), 2969-2974. doi: 10.3182/20140824-6-za-1003.01404
- [15] Ahmed, S., Ali, A., Joyo, M., Rehan, M., Siddiqui, F., & Bhatti, J. et al. (2018). Mobility assistance robot for disabled persons using electromyography (EMG) sensor. 2018 IEEE International Conference On Innovative Research And Development (ICIRD). doi: 10.1109/icird.2018.8376304
- [16] Sharmila, K., Sarath, T., & Ramachandran, K. (2016). EMG controlled low cost prosthetic arm. 2016 IEEE Distributed Computing, VLSI, Electrical Circuits And Robotics (DISCOVER). doi: 10.1109/discover.2016.7806239
- [17] Bronzino, J. (2006). *The biomedical engineering handbook* (3rd ed.). Boca Raton, FL [etc.]: CRC/Taylor & Francis.
- [18] Filtros Activos de Orden superior Pasa banda. (2019). Retrieved 9 November 2019, from <https://wilaebaelectronica.blogspot.com/2019/01/filtros-activos-de-orden-superior-pasa-banda.html>
- [19] Datasheet OP 07. <https://www.analog.com/media/en/technical-documentation/data-sheets/OP07.pdf>
- [20] Širok asortiman roba s područja elektronike i informatike - ElectronIC Center. (2020). From <https://electronic-center.hr/>

ANNEX 1

This table shows the approximation of Butterworth lowpass filter for orders superiors (2nd to 10th). The k_{LP} changes depending on the approximation used (in this case Butterworth is always 1) and the Q_{LP} means the quality factor on each stage.

Butterworth										
Order	Stage 1		Stage 2		Stage 3		Stage 4		Stage 5	
	k_{LP1}	Q_{LP1}	k_{LP2}	Q_{LP2}	k_{LP3}	Q_{LP3}	k_{LP4}	Q_{LP4}	k_{LP5}	Q_{LP5}
2	1.0000	0.7071	----	----	----	----	----	----	----	----
3	1.0000	1.0000	1.0000	----	----	----	----	----	----	----
4	1.0000	0.5412	1.0000	1.3065	----	----	----	----	----	----
5	1.0000	0.6180	1.0000	1.6182	1.0000	----	----	----	----	----
6	1.0000	0.5176	1.0000	0.7071	1.0000	1.9319	----	----	----	----
7	1.0000	0.5550	1.0000	0.8019	1.0000	2.2471	1.0000	----	----	----
8	1.0000	0.5098	1.0000	0.6013	1.0000	0.9000	1.0000	2.5628	----	----
9	1.0000	0.5321	1.0000	0.6527	1.0000	1.0000	1.0000	2.8785	1.0000	----
10	1.0000	0.5062	1.0000	0.5612	1.0000	0.7071	1.0000	1.1013	1.0000	3.1970